Western University

Scholarship@Western

Electrical and Computer Engineering Publications

Electrical and Computer Engineering Department

12-1-2023

Vertical Free-Swinging Photovoltaic Racking Energy Modeling: A Novel Approach To Agrivoltaics

Koami Soulemane Hayibo
Western University, khayibo@uwo.ca

Joshua M. Pearce
Western University, joshua.pearce@uwo.ca

Follow this and additional works at: https://ir.lib.uwo.ca/electricalpub

 Part of the Power and Energy Commons, Software Engineering Commons, and the Sustainability Commons

Citation of this paper:
Hayibo, Koami Soulemane and Pearce, Joshua M., "Vertical Free-Swinging Photovoltaic Racking Energy Modeling: A Novel Approach To Agrivoltaics" (2023). *Electrical and Computer Engineering Publications*. 602.
https://ir.lib.uwo.ca/electricalpub/602

Vertical Free-Swinging Photovoltaic Racking Energy Modelling: A Novel Approach to Agrivoltaics

Koami Soulemane Hayibo [1] and Joshua M. Pearce [1, 2, *]

[1] Department of Electrical & Computer Engineering, Western University, London, ON, Canada; khayibo@uwo.ca

[2] Ivey School of Business, Western University, London, ON, Canada

* Correspondence: Thompson Engineering Building, 1151 Richmond St. N., London, ON, Canada N6A 3K7; joshua.pearce@uwo.ca

Abstract

To enable lower-cost building materials, a free-swinging bifacial vertical solar photovoltaic (PV) rack has been proposed, which complies with Canadian building codes and is the lowest-capital-cost agrivoltaics rack. The wind force applied to the free-swinging PV, however, causes it to have a non-90° tilt angle and no energy performance model accurately describes such a system. To provide a simulation model for the free-swinging PV, where wind speed and direction govern the array tilt angle, this study builds upon the open-source System Advisor Model (SAM) using Python. After the SAM python model is validated, a view factor model is used to calculate front and back irradiations. The findings reveal that free-swinging PV generates 12% more energy than vertical fixed-tilt PV. Free-swinging PV offers a levelized racking cost, which is 30% lower than that of other agrivoltaics racks including commercial fixed-tilt metal, optimized fixed-tilt wood, and seasonally-adjusted wood PV racking.

1. Introduction

The cost of solar photovoltaic (PV) technology has plummeted, resulting in one of the lowest-cost electricity generation technologies available globally. Yet, far more work still needs to be done to replace all fossil fuels, not only in electricity generation, but also in transportation and heating (IEA et al., 2021; Palmer, 2019). At the current deployment rate of PV technologies worldwide (Cherp et al., 2021), humanity is not on track to limit negative consequences of energy-related climate change (Helveston et al., 2022). More solar PV is needed to reach the net zero carbon emissions goals of the United Nations (United Nations, 2023). One of the main challenges when integrating solar PV energy generation systems to power densely populated cities is land use conflict (Dias et al., 2019). In Japan, for example, a GIS analysis has revealed that the viable land for solar PV deployment will conflict with other development projects in 72% of the cases (Obane et al., 2020). A recent study has estimated that to enable an 80% solar PV penetration rate into the grid, 5% of the total land is required in the European Union, India, Japan, and South Korea (van de Ven et al., 2021). In a food-stressed environment, the public is reluctant to support conventional large-scale energy projects because they reduce the viable space used for agricultural food production (Roddis et al., 2020).

Recently, a new approach to solar PV called agrivoltaics offers a solution to these problems. Agrivoltaics refers to the co-location of PV and agricultural production and provides a particular promise in optimizing the food-water-energy nexus (Barron-Gafford et al., 2019). Agrivoltaics benefits documentation is ongoing in the literature. For example, agrivoltaics increases crop yield (Adeh et al., 2019), in addition to sustainable energy generation (Pearce, 2002) and greenhouse gas emission reduction (Barron-Gafford et al., 2019). Another advantage of agrivoltaics is the microclimate created by the solar panels, which shield the crops from excess solar irradiation (Adeh et al., 2019), preventing unnecessary water loss. This water loss

prevention contributes to water savings on agrivoltaics farmlands (Al-Saidi & Lahham, 2019). Past studies have argued that farmers that combine PV and agriculture have increased revenue and can maintain a better rural employment rate (Dinesh & Pearce, 2016). Additional potential benefits provided by agrivoltaics include better land use efficiency (Dupraz et al., 2011) and increased land productivity (Schindele et al., 2020), inflation hedging during high inflation periods and electricity generation for charging electric vehicles (Steadman & Higgins, 2022). In general, agrivoltaics is warmly received by the PV industry (Pascaris et al., 2021), the general public (Pascaris1 et al., 2021), and farmers (Pascaris et al., 2020). Farmers, however, want the minimal impact possible on their farming operation and the lowest-possible capital cost (Pascaris et al., 2020).

One area of PV systems where equipment costs have not decreased at the same rate as modules is PV racking (Feldman et al., 2021). Recent works on open-source development of racking designs have shown that PV costs could be reduced further by using alternative materials for agrivoltaics racks. Some alternative PV racking options explored in the literature that could be used for agrivoltaics systems involve using parking lot canopies to integrate with EV charging (Vandewetering et al., 2022c), existing wire fences (Hayibo & Pearce, 2022), solar PV wood-based fixed-tilt wooden PV racking (Vandewetering et al., 2022a), seasonally-adjusted wooden PV racking (Vandewetering et al., 2022b), and vertical free-swinging tilt wooden PV racking (Vandewetering et al., 2023). The vertical wood racking system is the most promising of these designs because it has the lowest capital cost (excluding the existing fencing concept that is limited in scaling potential) and would have minimal impact on conventional field crop agricultural operations. This is because rows of vertical racks can be spaced apart far enough to utilize existing farm equipment, which decreases inter-row shading (thus improving capacity factors) while only suffering from relatively minor increased conductivity losses from the longer wire runs needed when compared to a conventional industrial-scale PV farm.

This article further investigates the new design of vertical bifacial free-swinging agrivoltaics racks designed to be compliant with the Canadian building code. In addition, this study eliminates the previous assumption that the bifacial modules would remain vertical (90° tilt angle) during times of energy production (Vandewetering et al., 2023). The wind force applied to the free-swinging PV, will make non-90° tilt angles. After investigating the literature thoroughly, there is no energy performance model describing such a PV system where the tilt is determined by wind speed. Therefore, this study is the first to propose a simulation model for a bifacial vertical free-swinging PV where wind speed and direction govern the array tilt angle.

This simulation software used in this study builds upon the open-source System Advisor Model (SAM) energy performance software for a monofacial PV to provide a more accurate bifacial free-swinging PV energy performance model. The equations used to build SAM are converted into Python code and validated against SAM results. Then, a geometrical analysis is used to determine the view factors of the swinging bifacial PV. These view factors are used to calculate the solar irradiation incident on the front and back faces of the bifacial PV modules. The system energy output is estimated and compared to other PV systems, including a fixed-tilt vertical PV, an annually optimized tilt PV, and a seasonally adjusted PV. The energy results and the system cost are used to estimate the racking cost per watt and levelized cost of electricity (LCOE) of the racking. The results are discussed in the context of the synergies of vertical bifacial free-swinging PV with agriculture.

2. Methods

2.1. Proposed Bifacial Swinging PV Energy Model

The SAM model for fixed tilt monofacial system and the modifications needed to model the energy performance of the free-swinging PV are described in detail in the Supplementary Information (SI). The modifications focus on three aspects. First, the tracking of the hourly tilt angle and the system's azimuth as a function of wind speed, and wind direction. Then, the analysis of mutual shading between the three-layered solar modules on the rack. The third aspect is the top, middle and low modules view factors calculation. The view factors are useful to update the plane of array irradiance and ground-reflected irradiation values appropriate for the system.

2.1.1. Swinging Module Model Assumptions

The swinging PV model was built for hourly calculations. The average hourly steady state wind speed and wind direction were considered constant. As a result, the swinging PV tilt was also constant for each hour. The swinging movement of the PV modules were considered uniform; therefore, all PV modules have the same tilt angle. A bifaciality factor is applied to the irradiation reaching the back of the PV module. Additionally, if the sun is on the horizon in the early morning, the back side is considered to have an incident beam irradiation, and this effect is included for in the model. The ground-reflected irradiation on the back of a module is considered not highly affected by the module beneath it. This assumption considers there is enough space between two rows of swinging PV to minimize the impact of the bottom modules on the top rear ground-reflected irradiation.

2.1.2. Steady-State Wind Speed Conversion to Swinging PV Tilt

The first modification made to the SAM performance described in the Supplementary Information is the tilt angle calculation. The bifacial swinging PV racking is freely swinging; therefore, its tilt angle depends on the wind speed and wind direction. A free-body diagram with the module in static equilibrium is used to determine the tilt angle. The moment of the hinge caused by the wind force must equal the moment induced by the weight of the module. Figure 1 displays a free body diagram with the forces and their respective distances away from the hinge.

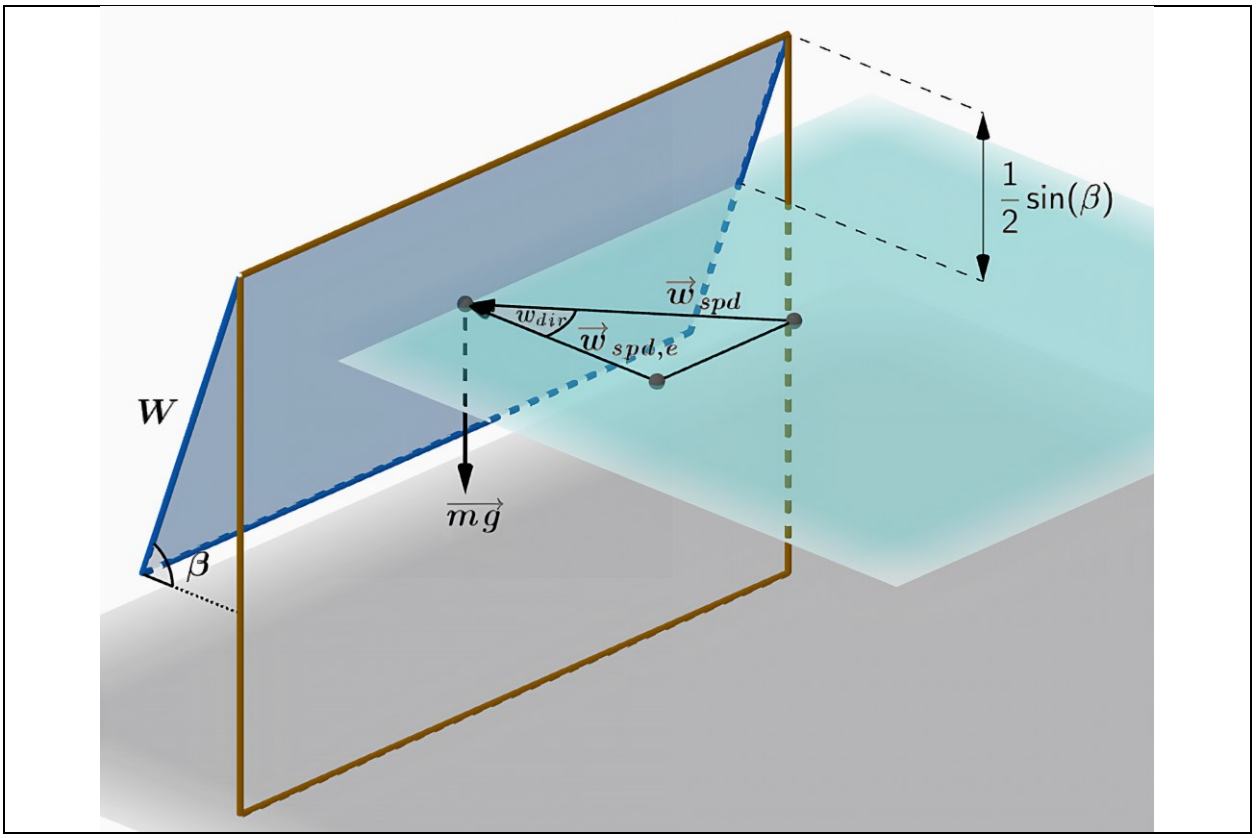

Figure 1. Free body diagram of a module subject to a wind force, F, and its own weight, m (Drawn in GeoGebra (Hohenwarter et al., 2023)).

Equation (4) is derived from the free body diagram equilibrium and it shows the relationship between the solar module tilt angle β (°), the effective wind speed $w_{spd,e}$ (m/s), and the drag coefficient C_D.

$$\frac{\cot(\beta)}{C_D \times \sin(\beta)} = \frac{\rho \times A_{PV} \times \left(w_{spd,e}\right)^2}{2 \times m \times g} \quad (1)$$

Where ρ (kg/m³) is the air density, A_{PV} (m²) is the surface area of the PV module, m (kg) is the module weight, and g (m/s²) is the gravitational acceleration.

The drag coefficient, C_D, varies based on the attack angle of the wind onto the module. Wind tunnel experimentation at Western University has provided accurate drag coefficients of PV modules for multiple different attack angles (Shademan & Hangan, 2009), which have been fit in the graph shown in Figure 2.

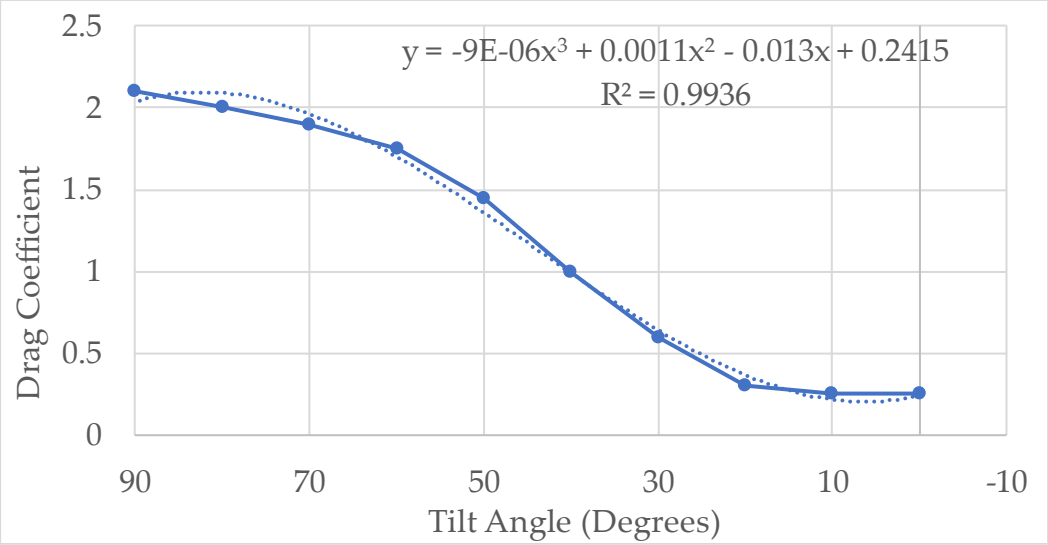

Figure 2. Experimental drag coefficients of PV modules for wind loads at varying tilt angles.

Equation (2) shows the interpolated equation between the tilt angle and the drag coefficient and equation (3) shows the impact of the wind direction w_{dir} (°) on the wind speed w_{spd} (m/s). γ_{surf} (°) is the surface azimuth that is adjusted here depending on the wind direction.

$C_D \simeq -0.000009\beta^3 + 0.0011\beta^2 - 0.013\beta + 0.2415$	(2)
$w_{spd,e} = w_{spd} \times \cos(w_{dir} - \gamma_{surf})$	(3)

Equation (1) is solved for each time step in the calculation to determine the hourly steady-state tilt of the PV module.

2.1.3. Modified Irradiation for Swinging Bifacial PV

Ray-tracing and view factors are the two most commonly used models in bifacial PV systems' performance evaluation (Appelbaum et al., 2019; Durusoy et al., 2020; Nassar, El-Khozondar, et al., 2022; Nassar, Belhaj, et al., 2022). View factors are preferred in the current study because the geometry of the system is constantly changing and using raytracing requires a high computation cost (Cumber, 2022)

Most past works on bifacial PV systems using view factors cover grounded-mounted PV systems (Appelbaum & Bany, 1979; Ayala Pelaez et al., 2020; Gilman et al., 2018; Liu & Jordan, 1963; Nassar, El-Khozondar, et al., 2022). The only study to cover vertical bifacial PV performance through view factors analyzes a fixed tilt overhang attached to a wall by Appelbaum et al. (Appelbaum et al., 2019). This study relies on the results of that one (Appelbaum et al., 2019) and develops a new model for freely swinging bifacial PV.

Shading and masking are two important effects that need to be quantified for bifacial swinging PV performance. Shading affects the direct beam irradiation, while masking affects diffuse irradiation (sky-diffuse and ground-reflected). The vertical PV design has four different irradiation surfaces that describe all three modules' front and back irradiation. The irradiation of the front side of the top collector G_{FT} (W/m²) is described in equation (4) and (5).

$G_{FT} = E_b \cos(\theta) + E_{dh} \times \left(V_f\right)_{top-sky}^{front} + a_g(E_b \cos(z) + E_{dh}) \times \left(V_f\right)_{top-ground}^{front}$	(4)
$\left(V_f\right)_{top-sky}^{front} = \frac{1+\cos(\beta)}{2}; \left(V_f\right)_{top-ground}^{front} = \frac{1-\cos(\beta)}{2}$	(5)

Where ρ is the ground albedo, and $\left(V_f\right)_{a-b}^{c}$ is the view factor between surface a and surface b and c is used here to designate whether the view factor is calculated for the front or the rear side of the modules. z (°) is the sun zenith angle, θ (°) the angle of incidence, E_b is the beam irradiation, E_{dh} is the diffuse irradiation, and a_g the ground albedo. The irradiation incident on the front side of the middle G_{FM} (W/m²) and bottom G_{FB} (W/m²) modules are the same due to the system geometry and the irradiation G_{MT} (W/m²) is shown in equations (6) and (7).

$G_{FM} = E_b \cos\theta + E_{dh} \times \left(V_f\right)_{middle-sky}^{front} + a_g(E_b \cos z + E_{dh}) \times \left(V_f\right)_{middle-ground}^{front}$	(6)
$\left(V_f\right)_{middle-sky}^{front} = \frac{CE+BE-BC}{2CE}; \left(V_f\right)_{middle-ground}^{front} = \frac{1-\cos(\beta)}{2}$	(7)

The irradiation incident on the rear side of the bottom module G_{RB} (W/m²) is calculated using equations (8) and (9). θ_{back} represents the angle of incidence during the sunrise when the sun is low on the horizon. It is the supplementary angle of the angle of incident θ.

$G_{RB} = E_b \cos(\theta_{back}) + E_{dh} \times \left(V_f\right)_{bottom-sky}^{rear} + a_g(E_b \cos(z) + E_{dh}) \times \left(V_f\right)_{bottom-ground}^{rear}$	(8)
$\left(V_f\right)_{bottom-sky}^{rear} = \frac{1-\cos(\beta)}{2}; \left(V_f\right)_{bottom-ground}^{rear} = \frac{1+\cos(\beta)}{2}; \theta_{back} = 180 - \theta$	(9)

The middle and top PV modules have the same rear irradiation G_{RM} (W/m²) and G_{RT} (W/m²). The middle and top modules' rear irradiation is calculated in the last position because, in addition to the beam, sky-diffuse, and ground-reflected irradiation, it also depends on the irradiation reflected by the front face of the collector below. Equations (10) to (13) show the calculation of the rear irradiation for the top and middle modules.

$G_{RT} = E_b \cos(\theta_{back}) + E_{dh} \times \left(V_f\right)_{top-sky}^{rear} + a_g(E_b \cos(z) + E_{dh}) \times \left(V_f\right)_{top-ground}^{rear} + a_{PV}^{sh} \times G_{FM} \times \left(V_f\right)_{top-(middleshaded)}^{rear} + a_{PV}^{un} \times G_{FM} \times \left(V_f\right)_{top-(middleunshaded)}^{rear}$	(10)
$\left(V_f\right)_{top-sky}^{rear} = \frac{1-cos\beta}{2}; \left(V_f\right)_{top-ground}^{rear} = \frac{1+cos\beta}{2}$	(11)
$\left(V_f\right)_{top-(middleshaded)}^{rear} = \frac{AD+BC-AC-BD}{2AB}$	(12)
$\left(V_f\right)_{top-(middleunshaded)}^{rear} = \frac{AE+BD-AD-BE}{AB}$	(13)

Where A, B, C, D, and E are points of the geometrical representation of two swinging PV modules as shown in Figure 3. a_{PV}^{sh} and a_{PV}^{un} are the reflection coefficient of the shaded PV glass, and the unshaded PV glass, respectively. The view factors calculations are detailed in Section 2.1.4.

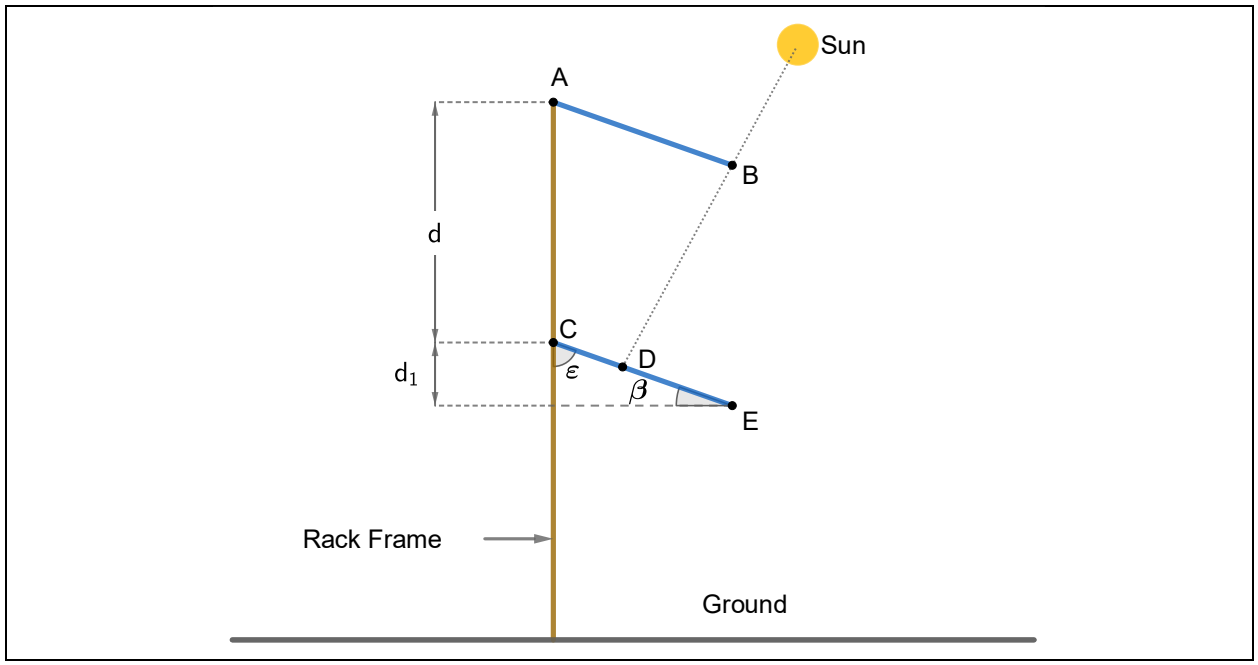

Figure 3. Graphical representation of the geometry of two swinging PV modules (Drawn in GeoGebra (Hohenwarter et al., 2023)).

2.1.4. Shading Analysis and View Factors Calculation Details

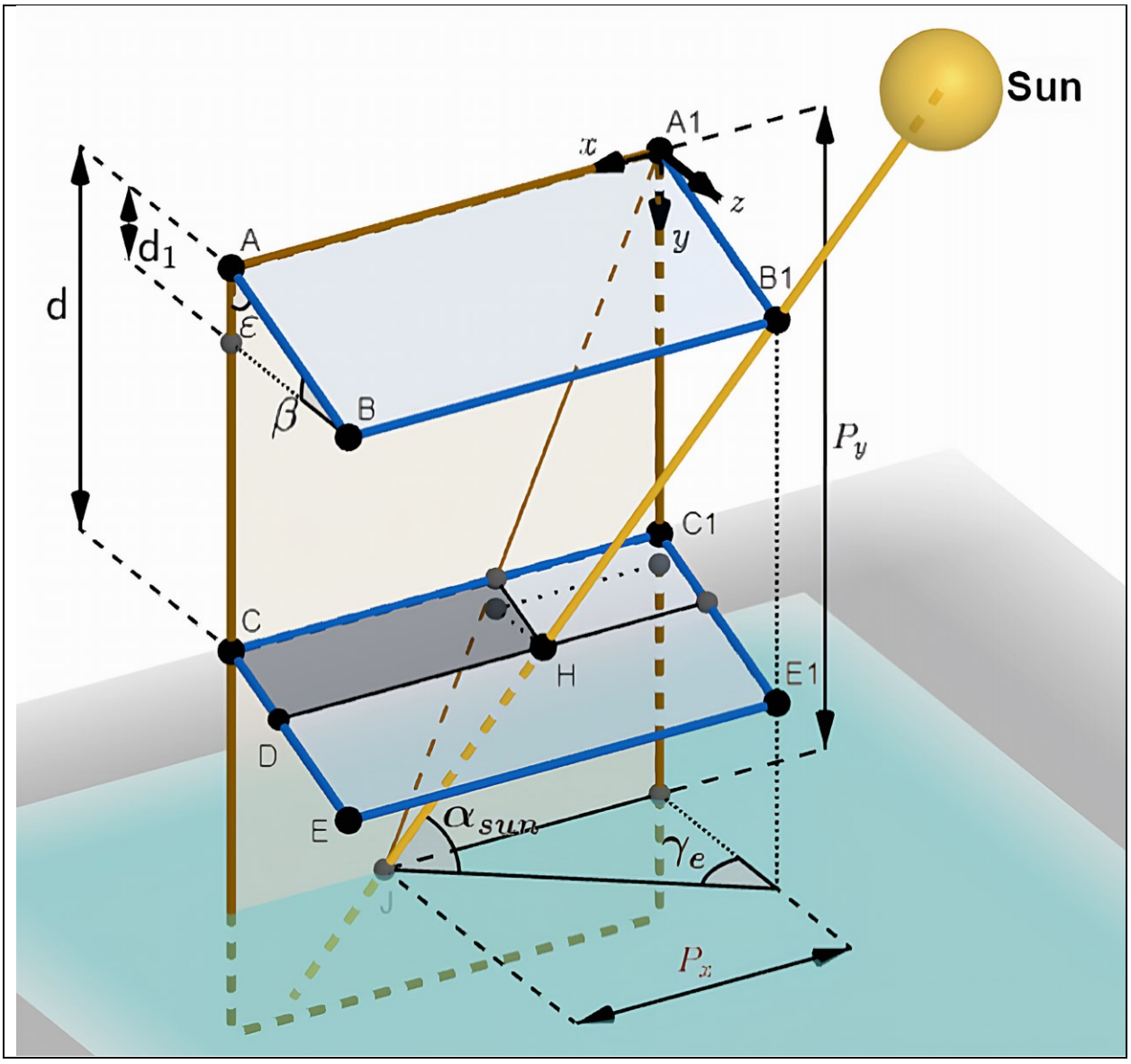

Figure 4. Three-dimensional representation of the two swinging PV modules for shading analysis (Drawn in GeoGebra (Hohenwarter et al., 2023))

Figure 4 shows a 3-D representation of the swinging PV systems. Two modules are shown for clarity, but it should be noted that the calculation performed can be applied to three or more modules. To find the shaded area cast by the top module on the bottom module, the coordinates (x_H, y_H, z_H) of point H are needed (see equation (14)).

$x_H = P_x \times \frac{y_H - d_1}{P_y - d_1} \quad ; \quad y_H = \frac{z_H}{\tan(\varepsilon)} + d \quad ; \quad z_H = W \sin(\varepsilon) \frac{P_y - d}{P_y - d1 + \frac{W \sin(\varepsilon)}{\tan(\varepsilon)}}$	(14)
$P_x = W \sin(\varepsilon) \tan(\gamma_e) \quad ; \quad P_y = W \cos(\varepsilon) + \frac{W \sin(\varepsilon)}{\cos(\gamma_e)} \tan(\alpha_{sun})$	(15)
$\varepsilon = 90 - \beta \quad ; \quad \gamma_e = \gamma_{surf} - \gamma_{sun}$	(16)

Where P_x and P_y are the coordinates of the shadow point H displacement in the (x, y) plane, W is the width of the PV module, d_1 is the projection of the module's width on the y-axis, d is the vertical distance between the hinges of two PV modules (PV width plus space between two PV modules when in resting position), ε is the displacement angle and is the complimentary angle of the swinging tilt angle, and γ_e is the effective azimuth that is the difference between the surface azimuth and the sun azimuth. The displacement of the shadow point H in the (x, y) plane is the point J that is the intersection of the sunlight with the plane of the racking frame.

The height S_h and length S_l of the shadow cast by the top module over the second module are calculated using equation (17). Equation (18) shows the calculation of the shaded area S_{area}. The shaded area is used to determine the DC beam irradiation shading loss factor in Section 2.1.5.

$S_h = \frac{y_H - d}{\cos(\varepsilon)} \quad ; \quad S_l = L - d \times \frac{P_x}{P_y}$	(17)
$S_{area} = S_h \times S_l$	(18)

The geometric calculation of the view factors is adapted from previous works (Appelbaum, 2018; Appelbaum & Bany, 1979). The segment in equations (7), (12), and (13) are calculated from the geometrical analysis and shown in equations (19) to (23)

$AD = \sqrt{(S_h \cos(\beta))^2 + (d + S_h \sin(\beta))^2}$	(19)
$BC = \sqrt{(d \cos(\beta))^2 + (d - W \sin(\beta))^2}$	(20)
$BD = \sqrt{(d \sin(\varepsilon))^2 + (W - d \cos(\varepsilon) + S_h)^2}$	(21)
$AE = d + W \sin(\beta)$	(22)
$BE = d \quad ; \quad AD = W$	(23)

2.1.5. Integration of the Bifacial Swinging PV View Factors to SAM Model

According to the irradiation equations derived in Section 2.1.3, the total irradiation on each of the modules is different depending on their position on the swinging rack. Therefore, the modules are considered as part of three different arrays, the top array, the middle array, and the bottom array. The front POA irradiation values for a monofacial PV (see Supplemental Information) are replaced by the equivalent front POA component calculated in equations (4) and (6). Each of these equations has a beam component, a diffuse component, and a ground-reflected component. Additionally, the rear POAs calculated in equations (8) and (10) are added to the total POA (see Supplemental Information). The rear POA values, however, are corrected by the bifaciality factor (Janssen et al., 2015) of the PV because the rear side of a bifacial PV generates less energy than the front side. The PV glass reflection coefficient used in the rear POA calculation is obtained from the transmission coefficient of the PV glass. The transmission coefficient calculation is detailed in the Sandia physical model for incident angle modifier (Sandia, 2022; Yamada et al., 2001). The simulation is run from the bottom array to the top array because the reflected irradiation at the front of the bottom arrays is used to calculate the irradiation on the rear of the top arrays.

Another important modification that was made to the SAM model is the application of the beam irradiation DC shading loss factor. This loss is considered in SAM, but only for ground-mounted fixed-tilt PV systems (Gilman et al., 2018). The beam irradiation shading factor is applied to the DC output instead of the beam POA because the bypass diodes in a solar module

block out the power from an entire string of PV cells, so even the diffuse energy irradiation incident on the shaded part is lost. In this study, the PV module is equipped with three bypass diodes defining three geometrical areas as shown in Figure 5. The shadow height calculated in equation (17) is compared with the module width and used to determine the portion of the PV that is unusable. For example, if the shadow height is more than one-third of the PV width, but less than two-thirds of the PV width, the loss factor is two-thirds or 66.67%. The DC loss factor is added to the system losses to find the DC power generation. The system losses are detailed in the Supplemental Information.

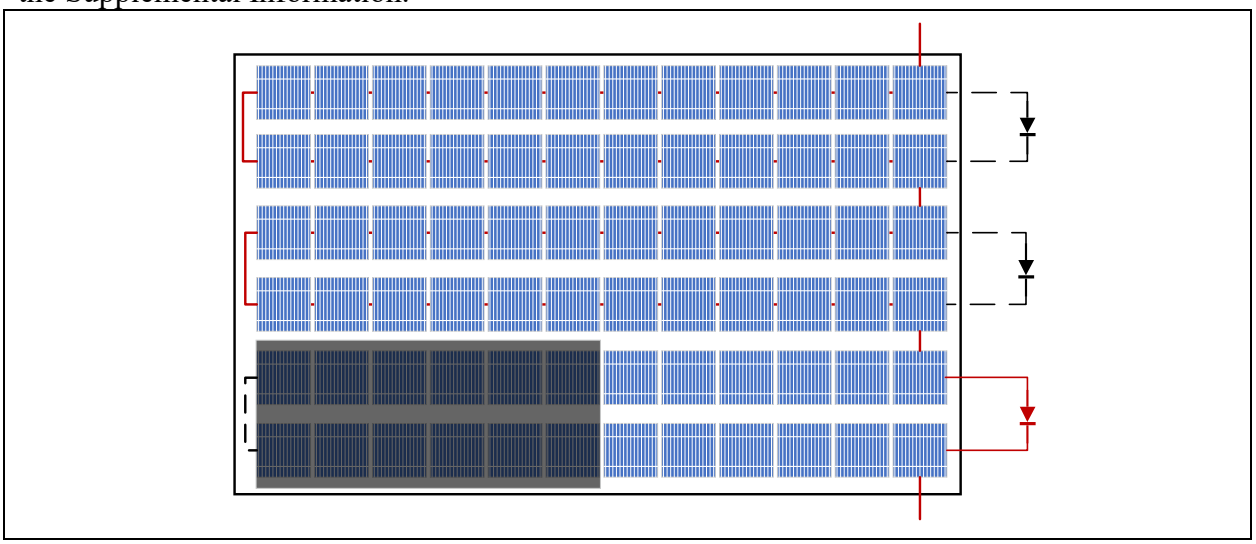

Figure 5. PV module showing the location of the by-pass diodes. The spaces between the cells are exaggerated for clarity. The dashed connection lines show the disconnections in the solar module.

The bifacial swinging PV energy performance model is implemented in Python (G. van Rossum (Guido), 1995) using Google Colab (Google, 2022). The implementation diagram is shown in Figure 6 and the code is available in an open-source repository (Hayibo & Pearce, 2023).

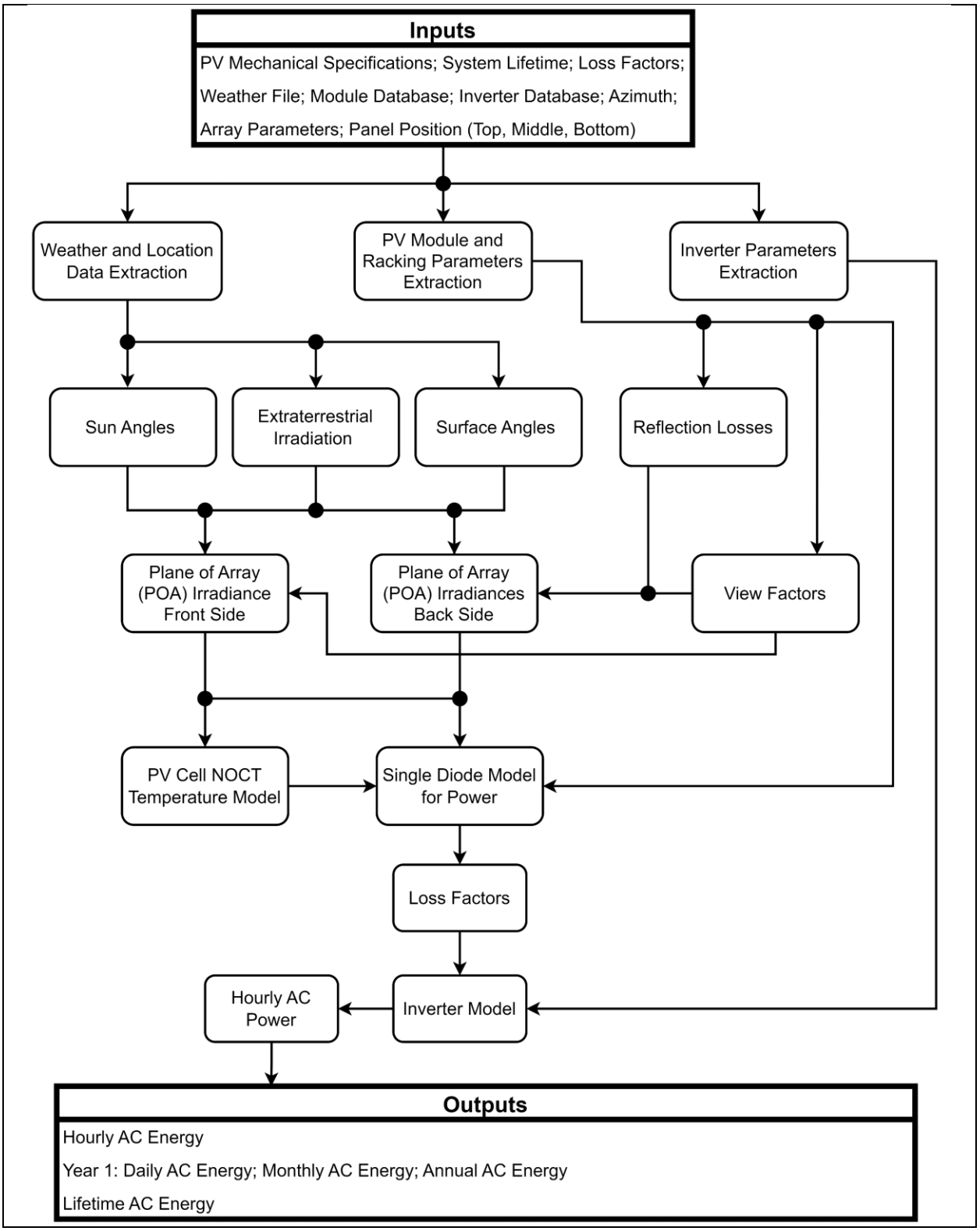

Figure 6. Step-by-step execution diagram of the bifacial swinging PV energy performance calculation.

2.2. Energy Performance Simulation

All the simulations performed in this study were hourly simulations. The first simulation performed was aimed at validating the monofacial fixed tilt performance model used by SAM. The code was run for three different locations using the latitude angle as the fixed tilt of the system, and the energy performance results were compared to SAM 2018 results, which are fully documented in the reference guide (Gilman et al., 2018). The three locations were London Ontario, Lomé Togo, and South Africa. These locations are chosen because they are respectively located in the northern hemisphere, close to the equator, and in the southern hemisphere, which thus provided a good range of optimal PV tilt angles. The simulation data used are shown in Table 1.

Table 1. Simulation data for the validation of the fixed tilt PV performance code.

Parameters	**London, Ontario**	**Lomé, Togo**	**South Africa**
Sky-diffuse Model	Isotropic Sky		
PV Module	SunPower SPR-X21-335		
Module Type	Mono Crystalline Silicon - Monofacial		
Number of Modules	18		
Inverter	SolarEdge Technologies: SE6000x		
Tilt Angle	34°	10°	25°
Azimuth (East of North)	180°	180°	0°
DC Power Rating	6.03 kWdc		
DC to AC Ratio	1.13		
Soiling Losses	5%		
DC Power Losses (SAM Default Values)	4.4%		
AC wiring Losses	1%		
Self-Shading	None		

After the code validation shown in the SI, a second set of simulations is run using the proposed bifacial swinging PV performance model. The simulation is performed with the geographical and weather data of London-Ontario (NREL-NSRDB, 2021). First, an azimuth optimization simulation was run using London-Ontario weather data. The azimuth was varied from 0° to 350° in 10° increments. The best azimuth value was used to simulate the swinging PV performance. The relationship between the effective wind speed, the tilt angle, and the azimuth was investigated. The energy performance during the first year of operation was compared to the performance of other bifacial PV systems, including a vertical metal racking fixed-tilt PV, an optimized wood racking fixed-tilt PV (Vandewetering et al., 2022a), and seasonally adjusted wood racking PV (Vandewetering et al., 2022b). A sensitivity analysis was conducted on the vertical distance between modules to analyze its impact on the system's performance. Table 2 shows the data used for the azimuth optimization and the comparison of the system.

Table 2. Simulation data for the azimuth optimization and different systems comparison

Parameters	**Swinging PV**	**Fixed Tilt Bifacial**	**Seasonally Adjusted Bifacial**

Location	London, Ontario		
Sky-diffuse Model	Isotropic Sky		
PV Module	Heliene 72M-400 G1 Bifacial		
Module Type	Mono Crystalline Silicon - Bifacial		
Bifaciality Factor	0.65		
Modules Per String	1		
Number of Strings	6		
Inverter	Altenergy Power System Inc : QS1A		
Tilt Angle	Depends on Wind Speed	34°	Seasonal (Vandewetering et al., 2022b)
Azimuth (East of North)	Best Azimuth from Optimization	180°	
DC Power Rating	2.4 kWdc		
DC to AC Ratio	1.58		
Soiling Losses	5%		
DC Power Losses (SAM Default Values)	4.4%		
AC Wiring Losses	1%		
Self-Shading	Yes	None	
System Lifetime	25 years		
PV Annual Degradation Rate	0.5%		

2.3. System Cost Analysis

The cost analysis of the bifacial swinging PV system expands on an existing study in which it was considered vertical with a 90° tilt angle during its operation (Vandewetering et al., 2023). Considering that the system is always at a 90° angle was a simplification due to the absence of an appropriate swinging PV energy performance model. The proposed model in this study accounts for the hourly tilt mangle change of the system, therefore allowing for a more accurate cost analysis.

The cost calculation of the swinging PV, including the tilt change, builds upon the methodology used in (Vandewetering et al., 2023). The cost analysis relied on the cost per Watt and the levelized cost of electricity ($LCOE_{rack}$). All the costs calculated in this study refer exclusively to the PV racking. The bifacial swinging PV system cost was compared to the cost of other wood racking systems (Vandewetering et al., 2022a, 2022b), and commercially available fixed-tilt vertical PV systems (Scharf et al., 2021).

3. Results

3.1. Azimuth Optimization Results of the Proposed Bifacial PV model

An azimuth optimization simulation was run to determine the optimal orientation of the bifacial swinging PV system, which depends on wind speed and direction whereas conventional PV systems depend only on the sun and shading. Figure 7 shows the results of the optimization. The maximum annual energy generation (2,702 kWh) happened at an azimuth of 260°, while the minimum energy generation (3,056 kWh) was at an azimuth of 170°. This optimization needs to be run with the wind data for each location where such an array is to be deployed. According to these findings, the best orientation for a bifacial swinging PV in the London-Ontario is an azimuth of 260°. This observation is slightly different compared to fixed-tilt vertical PV system.

In fixed-tilt vertical PV systems, the maximum annual energy generation occurs at either 90° or 270°. This difference is explained by the impact of the wind speed and direction on the swinging PV system.

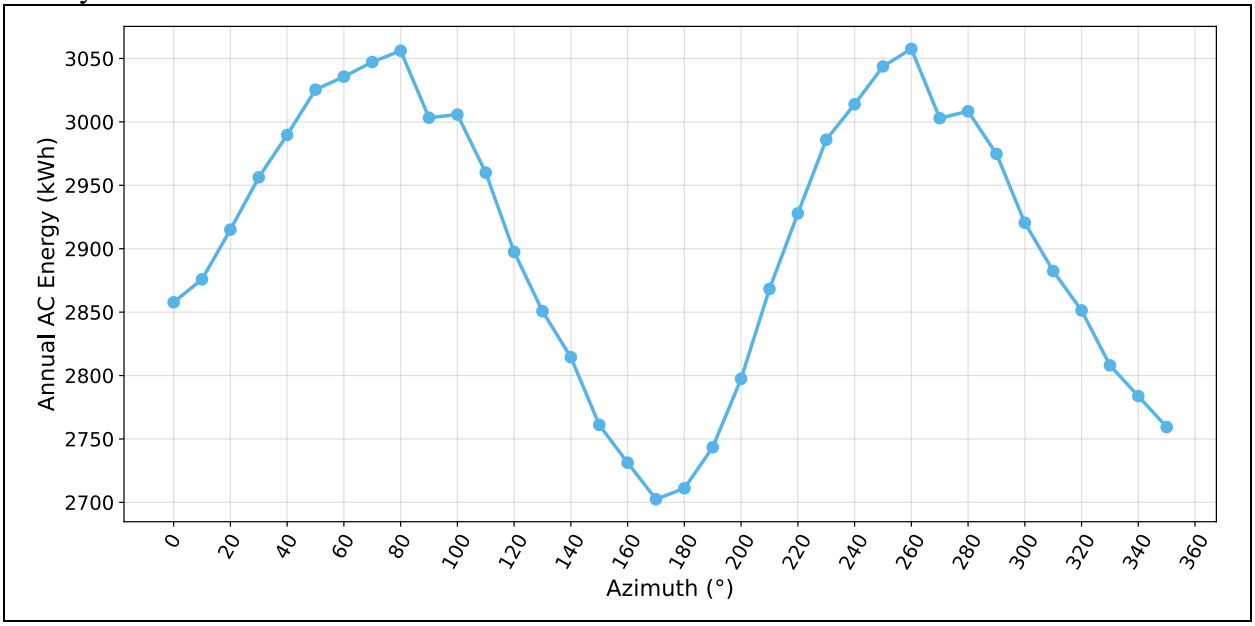

Figure 7. Azimuth angle optimization results of the swinging bifacial PV.

Figure 8 explores the relationship between the effective wind speed, the azimuth angle, and the tilt angle of the bifacial swinging PV system. The results in Figure 8 are obtained by performing a simulation of the bifacial energy performance using the optimal azimuth of 260°. In Figure 8a, the distribution of the effective wind speed shows a maximum of 10.7 m/s. This value implies that the maximum effective average wind force impacting the system will not exceed 12 m/s. This wind speed is much lower than the wind speed values for which the system was designed (40 m/s) (Vandewetering et al., 2023). The effective wind speed is less than 3.5 m/s in 75% of the cases. The effective wind load of the vertical system is much lower for the values it was designed for, potentially increasing the lifetime of the vertical racking system.

The results in Figure 8b reveal that the preferred orientation of the bifacial swinging PV system is an azimuth of 260°. This analysis is needed to determine how to install the swinging PV system. The two faces of a bifacial PV module generate different energy quantities. Explicitly, the back of the module produces less energy than the front. This difference in energy production is captured in the bifaciality factor provided by the module manufacturer (Janssen et al., 2015). Performing a simulation to determine the preferred azimuth of the system allows the PV module installation so that the front is facing the desired azimuth, therefore maximizing energy production. Figure 8b shows the tilt of the vertical swinging system as a function of the wind speed. At the maximum effective wind speed of 10.7 m/s, the tilt angle of the PV is 54.1°. The tilt angle is an important metric to determine the span or space occupation of the vertical swinging PV.

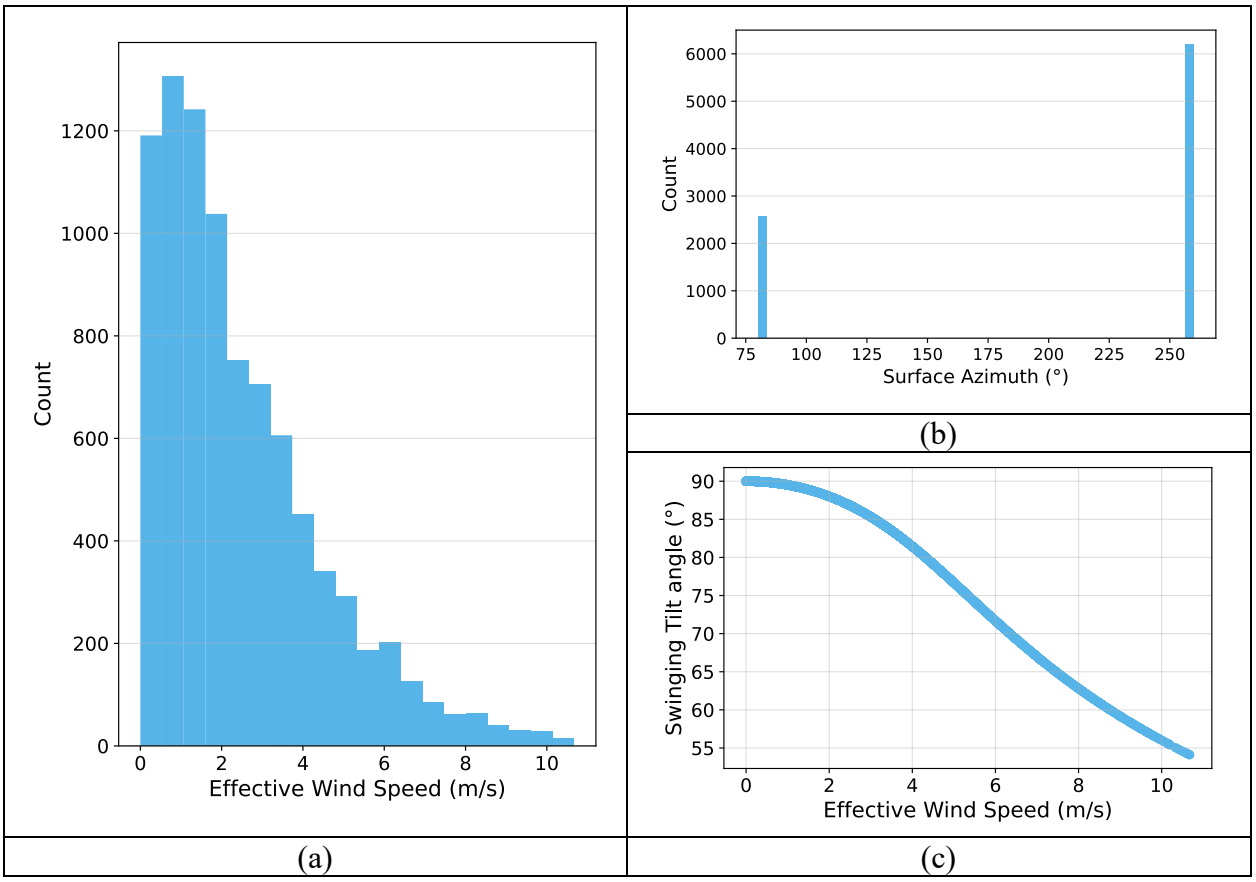

Figure 8. Plots of the effective wind speed, the surface azimuth, and swinging tilt angle for the optimal azimuth of 260°. (a) Distribution plot of the effective wind speed (m/s). (b) Distribution plot of the surface azimuth (°). (c) Scatter plot of the effective wind speed (m/s) and the swinging tilt angle (°).

3.2. Energy Performance Comparison to Existing PV Racking

Figure 9 compares the monthly energy performance of the vertical free-swinging PV system to a vertically fixed system, an annually optimized fixed tilt system, and a seasonally adjustable tilt system. The results are consistent across all months except for March. In March, the vertical swinging PV had a higher energy generation (288 kWh) than all the other systems, while the vertical fixed tilt had the lowest energy generation (242 kWh). A possible explanation for this observation is the swinging PV tilt angle in March, which allowed it to have a more optimal position than the other systems. This irregular boost in production shows how important wind speed is for the energy production of the swinging rack design. The seasonally variable PV always had the highest energy production, followed by the annually optimized fixed-tilt system for the remaining months. The vertical swinging PV consistently had the third highest energy production, and the vertical fixed tilt is the lowest energy generating system. The absolute percent difference between the vertical swinging PV and the seasonally variable tilt PV outside of March is between 5.8% and 27%. It should be noted that in March the wind was at the azimuth 260° most of the time, therefore the front was oriented towards the preferred side more often than in other months. This range of percent difference shows that the free-swinging bifacial

PV can potentially compete with existing systems, especially when the additional benefits of agrivoltaics are considered (Jamil et al., 2023).

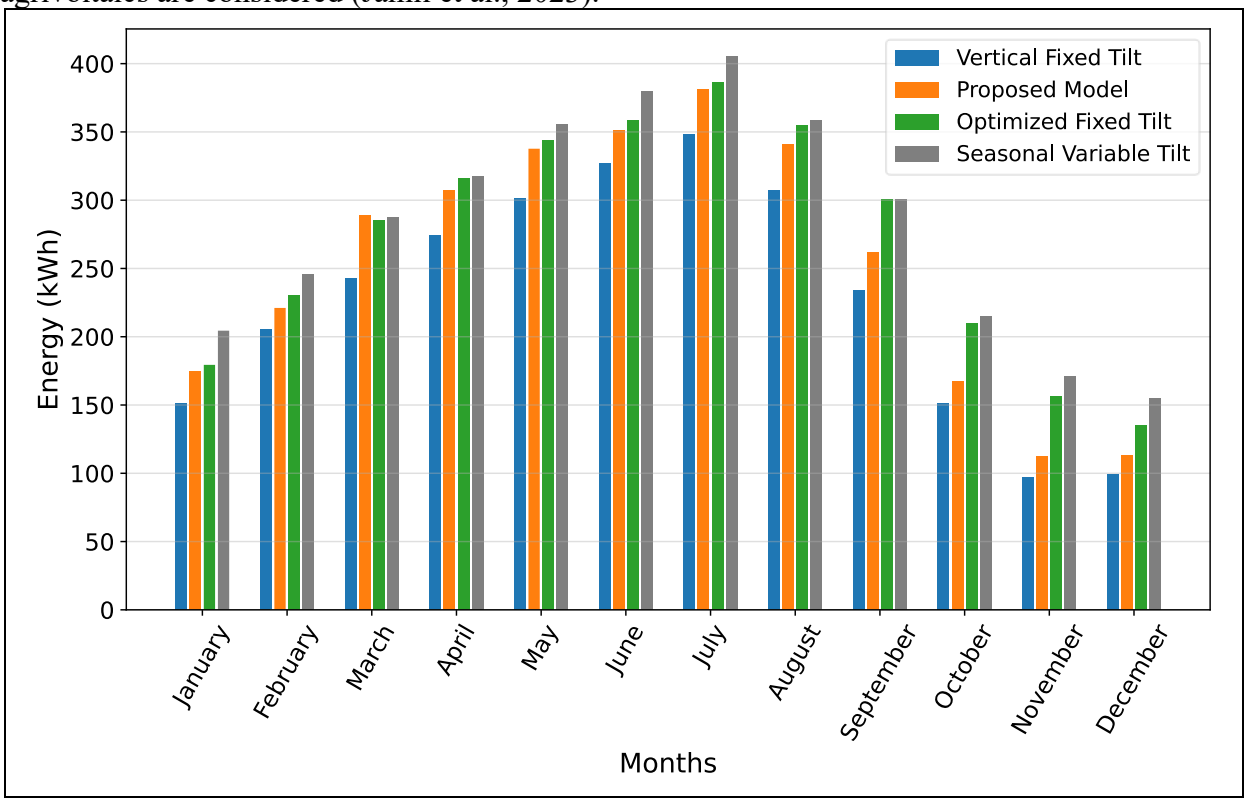

Figure 9. Comparison of the monthly energy production of the free-swinging PV to annually optimized fixed tilt PV, and seasonally variable tilt PV.

Figure 10 illustrates a detailed comparison of the two vertical PV systems using a percent difference analysis. According to the plotted data, for a given month, the swinging PV produced at least 7.4% more energy than the vertical fixed tilt and as much as 18.8% more. The swinging PV tilting caused by the wind force impact on the modules explains these observations.

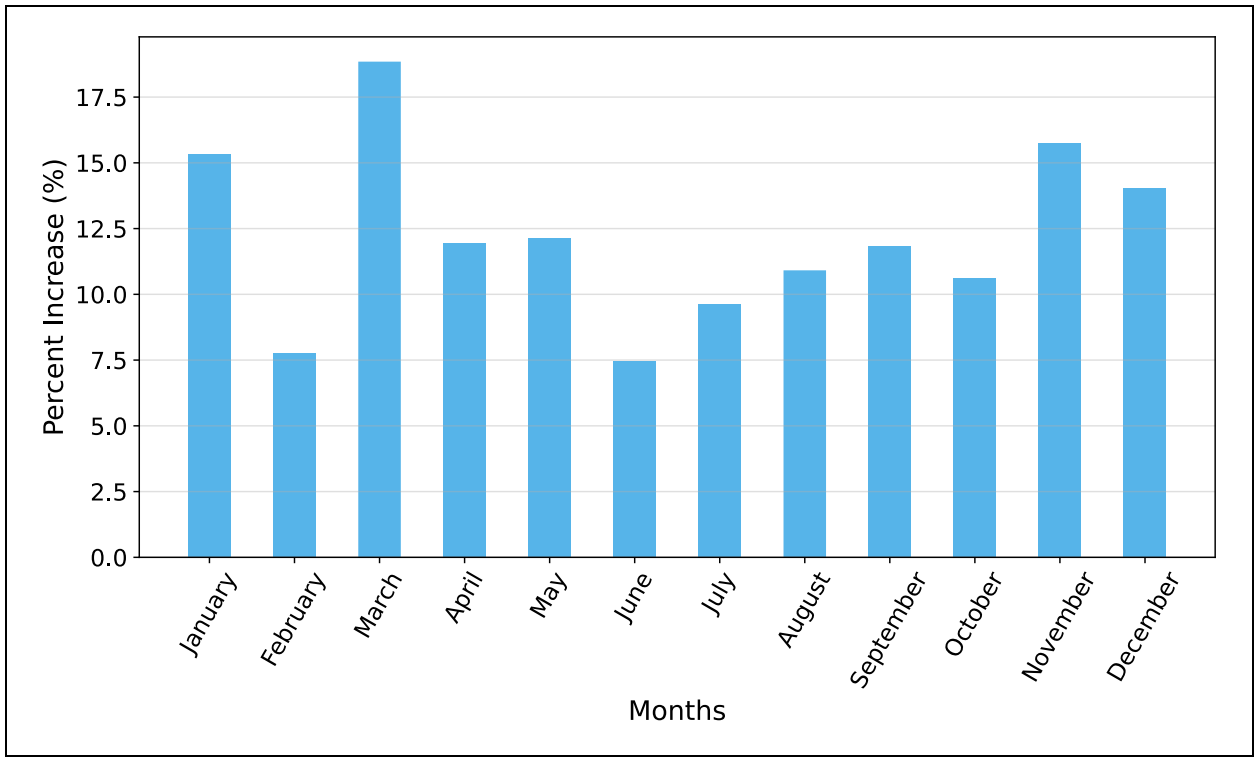

Figure 10. Detailed comparison of the two vertical systems showing the percent increase in monthly energy when switching from a fixed tilt vertical PV system to a free-swinging PV system. The increase is governed by both wind velocity and azimuth.

One of the limiting factors of the energy generation of the bifacial swinging PV is the vertical distance between modules. The vertical distance between the module (0.2 m) used in this study originates from the original design (Vandewetering et al., 2023). Thus, the modules cause self-shading on one another when the wind blows them out of vertical, resulting in the system energy performance reduction from a single module case. This reduction can limit the system performance when the wind force makes the module tilt towards the horizontal plane in the middle of the day during the summer. Figure 11 presents the impact of increasing the distance between modules on the system's energy performance. The data reveals that when the distance between the modules increases, the energy performance follows as expected. For example, if the distance between modules is 1m, the swinging PV generates more energy than an optimized tilt PV. Similarly, if the distance is 1.8m, the bifacial system performs better than a seasonally adjusted tilt PV. The reduction of self-shading between modules explains the boost in energy reported when the distance between modules increases.

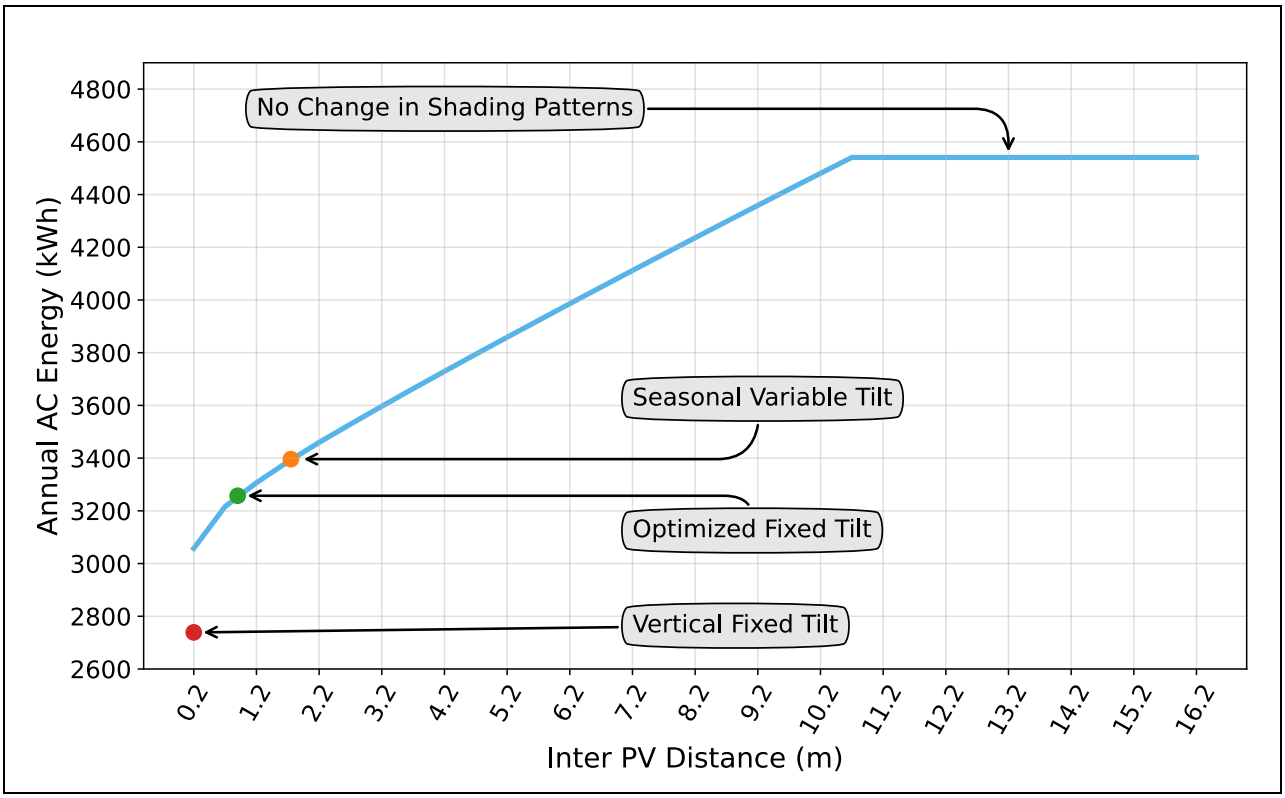

Figure 11. Variation of the annual energy production of the swinging PV when the space between modules is increased. The results are compared with a vertical fixed tilt PV, an optimized fixed tilt PV, and a seasonally variable tilt PV. The knee-point before the plateau shows the minimum vertical distance from where the shading losses remain the same and increasing the vertical distance between PV does not improve the energy performance.

3.3.Economic Analysis Results

Table 3 compares the cost of the vertical swinging PV to the cost of other systems. The fixed tilt and seasonal tilt wood racking have higher lifetime energy generation values when compared to the vertical systems. The vertical systems, however, have a lower cost per racking and racking LCOE. Specifically, the free-swinging vertical PV shows the lowest racking cost per unit power (CAD$0.21/W) and the lowest racking LCOE (CAD$0.0065/kWh). An LCOE of CAD$0.0065/kWh) is an 12% cost reduction compared to the cost of the free-swinging wood PV (CAD$0.0073/kWh) when the modules were always considered vertical at a tilt angle of 90° for the same location (Vandewetering et al., 2023). The lifetime energy of the swinging PV system is 12% higher than the energy generated by a fixed-tilt vertical system. This outcome confirms that the movement of the modules induced by the wind force benefits the overall performance of the system in addition to reducing the wind load on the structural elements which enables lower material costs and alternative materials like wood. According to the cost comparison in Table 3, the free-swinging bifacial wood-racking PV system offers the lowest racking cost in PV systems to date.

Table 3. Cost comparison of the proposed racking system and a commercial racking system

Racking System (2.4 kW)	**Racking Cost per Watt**	**Racking Cost**	**Lifetime Energy**	**Racking LCOE**

	(CAD$/W)	(CAD$)	(kWh)	(CAD$/kWh)
Wood Optimized Fixed Tilt (Vandewetering et al., 2022a)	$0.32	$768.00	80,130	$0.0096
Wood Seasonal Tilt (Vandewetering et al., 2022b)	$0.34	$816.00	84,304	$0.0097
Commercial Metal Vertical Fixed Tilt [1] (Scharf et al., 2021)	$0.27	$656.00	68,940	$0.0095
Free Swinging Vertical Wood Racking (this study)	$0.21	$505.08	77,404	$0.0065

[1] The racking cost per watt of the commercial vertical tilt was originally in Euros and converted to CAD with the rate of June 5, 2022 (1 Euro = 1.35 CAD) (Google Finance, 2023).

4. Discussion

Collectively, the findings in this study imply that vertical free-swinging PV could offer the best racking economics for agrivoltaics PV systems to date. It has the lowest price of documented agrivoltaics racking in terms of cost per Watt and levelized cost of electricity of the rack. In addition to the cost savings, the free-swinging PV offers a high specific energy yield compared to a fixed-tilt PV racking. The swinging PV specific energy during the first year of operation is 1,274 kWh/kW, while the specific energy of a fixed tilt vertical PV is 1,141 kWh/kW. Thus, using a free-swinging PV rack instead of a vertical fixed-tilt rack boosts the specific energy yield of an agrivoltaics system installed in London-Ontario by 12%.

According to the results, the best orientation of a bifacial free-swinging PV system could differ from the best orientation of other bifacial PV systems, depending on the location. More specifically, the azimuth optimization analysis shows that the best orientation for a swinging PV in London-Ontario is an azimuth of 260°. Meanwhile, the best azimuth in the same city is 90° (or 270°) and 180° for a vertical fixed-tilt and an optimized tilt PV, respectively. An azimuth optimization simulation appears crucial to determine the best orientation that allows the system to harvest the maximum power. This optimization would need to be coupled with statistical wind speed analysis to predict the long-term behavior of the wind and to determine the best azimuth for the lifetime of the swinging PV. The results have similarly shown a dependency between the PV tilt and the wind speed. This dependency makes the free-swinging PV a hybrid renewable energy system that uses wind and solar to generate the most energy. This dependency is also crucial to optimize the minimum safety spacing around an array on an agrivoltaics farmland.

This study focuses on the energy performance of a single row of free-swinging bifacial PV. On agrivoltaics farmlands using small equipment (e.g. short boom lengths), however, multiple close-packed rows could cast shade on one another, depending on the crop-dependent farm configuration. Therefore, additional studies are needed to determine the impact of row positioning and orientation on the energy performance of an agrivoltaics vertical swinging PV. Wind speed variation can also impact the optimal azimuth of swinging PV. Here the wind speed was in steady-state for every hour of the study. Yet wind speed is continuously variable. To account for this variability, future studies must investigate the dynamic energy performance using a real-time tilt angle variation. This investigation could be performed by collecting field data or data in a wind tunnel with sensors or computer vision-based monitoring. An added step worth considering in future studies, while using real-time wind speed for the energy performance calculation, is the collection of stress applied on the hinges and wooden beams of the bifacial

free-swinging PV. This field data analysis could potentially enable an additional reduction in the cross-section of mechanical members, leading to the concurrent reductions in embodied energy and materials. Therefore, further decreasing the overall cost of the racking. Also, the stress data collected could be beneficial in conducting a finite element analysis of the swinging rack structural design. The data can be valuable to ensure that both hinges and wires are not abraded over a long time period. One key aspect to consider with swinging PV governed by wind speed is the fluctuations the swinging movement could induce in the electrical system. Further studies are required to explore PV controller and inverter behavior when connected to a swinging PV. The cost analysis in this study was focused on the racking. Future studies could use field data to run a detailed cost and energy production analysis. The results could be used in comparing the LCOE and lifecycle environmental impacts of the entire swinging PV system to existing PV technologies. Another promising area of further research is the design of PV modules that are optimized for swinging PV racks, such as PV modules using lighter frames (Sadat et al., 2022) or with built-in coupling hinges. In addition, future work could investigate the best position of bypass diodes to provide an additional optimization step to the vertical swinging-ready PV module.

The results of this study could improve the prospecting of agrivoltaics PV sites. The dependency of the PV energy performance on the wind speed offers an opportunity for the windiest farming areas to be the most suitable for swinging PV. Future studies could use existing wind maps to build swinging PV energy performance maps for different locations across the globe. Particularly, adding swing-PV agrivoltaics installation on farms with wind farms may enable a symbiotic use of electrical infrastructure, which needs to be investigated. The swinging PV maps could extend to the statistical analysis of dependencies between the swinging PV energy performance and the wind profile using machine learning.

5. Conclusions

This study is the first to propose an energy performance model for free-swinging bifacial PV systems. The model was built on the existing SAM energy performance using empirical view factors analysis and is made freely available under a GNU General Public License. The results emphasize the importance of wind speed and direction of free-swinging PV energy generation. The findings reveal that free-swinging PV generates 12% more energy than vertical fixed-tilt PV systems for a case study location in an agricultural center in Canada. Free-swinging PV offers the lowest cost per watt (CAD$0.21/W) and LCOE (CAD$0.007/kWh) for agrivoltaics racking to date. More specifically, the LCOE of swinging PV is at least 31% lower than the LCOE of commercial fixed-tilt metal racking, optimized fixed-tilt wood racking PV, and seasonally adjusted wood racking PV. The results presented here offer an opportunity to study solar PV systems in a new light by integrating wind speed into the energy performance modeling of PV systems.

6. References

Adeh, E. H., Good, S. P., Calaf, M., & Higgins, C. W. (2019). Solar PV Power Potential is Greatest Over Croplands. *Scientific Reports*, *9*(1), 11442. https://doi.org/10.1038/s41598-019-47803-3

Al-Saidi, M., & Lahham, N. (2019). Solar energy farming as a development innovation for vulnerable water basins. *Development in Practice*, *29*(5), 619–634. https://doi.org/10.1080/09614524.2019.1600659

Appelbaum, J. (2018). The role of view factors in solar photovoltaic fields. *Renewable and Sustainable Energy Reviews*, *81*, 161–171. https://doi.org/10.1016/j.rser.2017.07.026

Appelbaum, J., Aronescu, A., & Maor, T. (2019). Shading by Overhang PV Collectors. *Applied Sciences*, *9*(20), Article 20. https://doi.org/10.3390/app9204280

Appelbaum, J., & Bany, J. (1979). Shadow effect of adjacent solar collectors in large scale systems. *Solar Energy*, *23*(6), 497–507. https://doi.org/10.1016/0038-092X(79)90073-2

Ayala Pelaez, S., Deline, C. A., Marion, W. F., Sekulic, W. R., & Stein, J. S. (2020). *Understanding Bifacial PV Modeling: Raytracing and View Factor Models* (NREL/PR-5K00-75628). National Renewable Energy Lab. (NREL), Golden, CO (United States). https://www.osti.gov/biblio/1597241

Barron-Gafford, G. A., Pavao-Zuckerman, M. A., Minor, R. L., Sutter, L. F., Barnett-Moreno, I., Blackett, D. T., Thompson, M., Dimond, K., Gerlak, A. K., Nabhan, G. P., & Macknick, J. E. (2019). Agrivoltaics provide mutual benefits across the food–energy–water nexus in drylands. *Nature Sustainability*, *2*(9), 848–855. https://doi.org/10.1038/s41893-019-0364-5

Cherp, A., Vinichenko, V., Tosun, J., Gordon, J. A., & Jewell, J. (2021). National growth dynamics of wind and solar power compared to the growth required for global climate targets. *Nature Energy*, *6*(7), Article 7. https://doi.org/10.1038/s41560-021-00863-0

Cumber, P. S. (2022). View factors-when is ray tracing a good idea? *International Journal of Heat and Mass Transfer*, *189*, 122698. https://doi.org/10.1016/j.ijheatmasstransfer.2022.122698

Dias, L., Gouveia, J. P., Lourenço, P., & Seixas, J. (2019). Interplay between the potential of photovoltaic systems and agricultural land use. *Land Use Policy*, *81*, 725–735. https://doi.org/10.1016/j.landusepol.2018.11.036

Dinesh, H., & Pearce, J. M. (2016). The potential of agrivoltaic systems. *Renewable and Sustainable Energy Reviews*, *54*, 299–308. https://doi.org/10.1016/j.rser.2015.10.024

Dupraz, C., Marrou, H., Talbot, G., Dufour, L., Nogier, A., & Ferard, Y. (2011). Combining solar photovoltaic panels and food crops for optimising land use: Towards new agrivoltaic schemes. *Renewable Energy*, *36*(10), 2725–2732. https://doi.org/10.1016/j.renene.2011.03.005

Durusoy, B., Ozden, T., & Akinoglu, B. G. (2020). Solar irradiation on the rear surface of bifacial solar modules: A modeling approach. *Scientific Reports*, *10*(1), Article 1. https://doi.org/10.1038/s41598-020-70235-3

Feldman, D., Ramasamy, V., Fu, R., Ramdas, A., Desai, J., & Margolis, R. (2021). *U.S. Solar Photovoltaic System and Energy Storage Cost Benchmark: Q1 2020* (Technical Report NREL/TP-6A20-77324; p. 120). National Renewable Energy Laboratory. https://www.nrel.gov/news/program/2021/documenting-a-decade-of-cost-declines-for-pv-systems.html

G. van Rossum (Guido). (1995). Python reference manual. In *Department of Computer Science [CS]* (Issue R 9525). CWI. https://ir.cwi.nl/pub/5008

Gilman, P., DiOrio, N. A., Freeman, J. M., Janzou, S., Dobos, A., & Ryberg, D. (2018). *SAM Photovoltaic Model Technical Reference 2016 Update* (Technical Report NREL/TP-6A20-67399; p. 93). National Renewable Energy Lab. (NREL), Golden, CO (United States). https://doi.org/10.2172/1429291

Google. (2022, January 18). *Google Colaboratory* [Software]. Google Colab. https://colab.research.google.com/?utm_source=scs-index

Google Finance. (2023, January 15). *EUR/CAD Currency Exchange Rate & News—Google Finance* [Finance]. Euro to Canadian Dollar. https://www.google.com/finance/quote/USD-CAD

Hayibo, K. S., & Pearce, J. M. (2022). Optimal inverter and wire selection for solar photovoltaic fencing applications. *Renewable Energy Focus*, *42*, 115–128. https://doi.org/10.1016/j.ref.2022.06.006

Hayibo, K. S., & Pearce, J. M. (2023). Vertical Free-Swinging Photovoltaic Racking Energy Modelling—Data and Performance Code. *Open Science Framework*. https://osf.io/jhx4b/

Helveston, J. P., He, G., & Davidson, M. R. (2022). Quantifying the cost savings of global solar photovoltaic supply chains. *Nature*, *612*(7938), Article 7938. https://doi.org/10.1038/s41586-022-05316-6

Hohenwarter, M., Borcherds, M., Ancsin, G., Bencze, B., Blossier, M., Éliás, J., Frank, K., Gál, L., Hofstätter, A., Jordan, F., Konečný, Z., Kovács, Z., Lettner, E., Lizelfelner, S., Parisse, B., Solyom-Gecse, C., Stadlbauer, C., & Tomaschko, M. (2023, January). *GeoGebra 5.0.507.0* [Software]. Geogebra 3D Calculator. https://www.geogebra.org/3d

IEA, Bouckaert, S., Pales, A. F., McGlade, C., Remme, U., Wanner, B., Varro, L., D'Ambrosio, D., & Spencer, T. (2021). *Net Zero by 2050: A Roadmap for the Global Energy Sector* (p. 224) [Publication]. International Energy Agency. https://trid.trb.org/view/1856381

Jamil, U., Bonnington, A., & Pearce, J. M. (2023). The Agrivoltaic Potential of Canada. *To Be Published*.

Janssen, G. J. M., Van Aken, B. B., Carr, A. J., & Mewe, A. A. (2015). Outdoor Performance of Bifacial Modules by Measurements and Modelling. *Energy Procedia*, *77*, 364–373. https://doi.org/10.1016/j.egypro.2015.07.051

Liu, B. Y. H., & Jordan, R. C. (1963). The long-term average performance of flat-plate solar-energy collectors: With design data for the U.S., its outlying possessions and Canada. *Solar Energy*, *7*(2), 53–74. https://doi.org/10.1016/0038-092X(63)90006-9

Nassar, Y. F., Belhaj, S., Alsadi, S. Y., & El-Khozondar, H. J. (2022). Analysis of the View Factors in Rooftop PV Solar. *2022 3rd International Conference on Smart Grid and Renewable Energy (SGRE)*, 1–6. https://doi.org/10.1109/SGRE53517.2022.9774104

Nassar, Y. F., El-Khozondar, H. J., Belhaj, S. O., Alsadi, S. Y., & Abuhamoud, N. M. (2022). View Factors in Horizontal Plane Fixed-Mode Solar PV Fields. *Frontiers in Energy Research*, *10*. https://www.frontiersin.org/articles/10.3389/fenrg.2022.859075

NREL-NSRDB. (2021, January 21). *National Solar Radiation Database* [Data]. NSRDB. https://nsrdb.nrel.gov/

Obane, H., Nagai, Y., & Asano, K. (2020). Assessing land use and potential conflict in solar and onshore wind energy in Japan. *Renewable Energy*, *160*, 842–851. https://doi.org/10.1016/j.renene.2020.06.018

Palmer, G. (2019). Renewables rise above fossil fuels. *Nature Energy*, *4*(7), Article 7. https://doi.org/10.1038/s41560-019-0426-y

Pascaris, A. S., Schelly, C., Burnham, L., & Pearce, J. M. (2021). Integrating solar energy with agriculture: Industry perspectives on the market, community, and socio-political dimensions of agrivoltaics. *Energy Research & Social Science*, *75*, 102023. https://doi.org/10.1016/j.erss.2021.102023

Pascaris, A. S., Schelly, C., & Pearce, J. M. (2020). A First Investigation of Agriculture Sector Perspectives on the Opportunities and Barriers for Agrivoltaics. *Agronomy*, *10*(12), Article 12. https://doi.org/10.3390/agronomy10121885

Pascaris1, A. S., Schelly, C., Rouleau, M., & Pearce, J. M. (2021). *Do Agrivoltaics Improve Public Support for Solar Photovoltaic Development? Survey Says: Yes!* [Preprint]. SocArXiv. https://doi.org/10.31235/osf.io/efasx

Pearce, J. M. (2002). Photovoltaics—A path to sustainable futures. *Futures*, *34*(7), 663–674. https://doi.org/10.1016/S0016-3287(02)00008-3

Roddis, P., Roelich, K., Tran, K., Carver, S., Dallimer, M., & Ziv, G. (2020). What shapes community acceptance of large-scale solar farms? A case study of the UK's first 'nationally significant' solar farm. *Solar Energy*, *209*, 235–244. https://doi.org/10.1016/j.solener.2020.08.065

Sadat, S. A., Vandewetering, N., & Pearce, J. M. (2022). *Mechanical and economic analysis of conventional aluminum photovoltaic module frames, frames with side holes, and open-source downward-fastened frames for non-traditional racking*. OSF Preprints. https://doi.org/10.31219/osf.io/uts48

Sandia. (2022, December 26). PV Performance Modeling Collaborative | Physical IAM Model [Research Institute]. *PV Perofrmance Modeling Collaborative*. https://pvpmc.sandia.gov/modeling-steps/1-weather-design-inputs/shading-soiling-and-reflection-losses/incident-angle-reflection-losses/physical-model-of-iam/

Scharf, J., Grieb, M., & Fritz, M. (2021). Agri-Photovoltaik Stand und offene Fragen. *Technologie-Und Förderzentrum Im Kompetenzzentrum Für Nachwachsende Rohstoffe. Straubing (Berichte Aus Dem TFZ, 73). Online Verfügbar Unter Https://Www. Tfz. Bayern. de/Mam/Cms08/Rohstoff Pflanzen/Dateien/Tfz_bericht_73_agri-Pv. Pdf, Zuletzt Geprüft Am*, *19*, 2021.

Schindele, S., Trommsdorff, M., Schlaak, A., Obergfell, T., Bopp, G., Reise, C., Braun, C., Weselek, A., Bauerle, A., Högy, P., Goetzberger, A., & Weber, E. (2020). Implementation of agrophotovoltaics: Techno-economic analysis of the price-performance ratio and its policy implications. *Applied Energy*, *265*, 114737. https://doi.org/10.1016/j.apenergy.2020.114737

Shademan, M., & Hangan, H. (2009). Wind loading on solar panels at different inclination angles. *11th Americas Conference on Wind Engineering*, 22–26.

Steadman, C. L., & Higgins, C. W. (2022). Agrivoltaic systems have the potential to meet energy demands of electric vehicles in rural Oregon, US. *Scientific Reports*, *12*(1), Article 1. https://doi.org/10.1038/s41598-022-08673-4

United Nations. (2023, January 23). *Net Zero Coalition* [International Organization]. Climate Action; United Nations. https://www.un.org/en/climatechange/net-zero-coalition

van de Ven, D.-J., Capellan-Peréz, I., Arto, I., Cazcarro, I., de Castro, C., Patel, P., & Gonzalez-Eguino, M. (2021). The potential land requirements and related land use change emissions of solar energy. *Scientific Reports*, *11*(1), Article 1. https://doi.org/10.1038/s41598-021-82042-5

Vandewetering, N., Hayibo, K. S., & Pearce, J. M. (2022a). Impacts of Location on Designs and Economics of DIY Low-Cost Fixed-Tilt Open Source Wood Solar Photovoltaic Racking. *Designs*, *6*(3), 41. https://doi.org/10.3390/designs6030041

Vandewetering, N., Hayibo, K. S., & Pearce, J. M. (2022b). Open-Source Design and Economics of Manual Variable-Tilt Angle DIY Wood-Based Solar Photovoltaic Racking System. *Designs*, *6*(3), Article 3. https://doi.org/10.3390/designs6030054

Vandewetering, N., Hayibo, K. S., & Pearce, J. M. (2022c). Open-Source Photovoltaic—Electrical Vehicle Carport Designs. *Technologies*, *10*(6), Article 6. https://doi.org/10.3390/technologies10060114

Vandewetering, N., Hayibo, K. S., & Pearce, J. M. (2023). Open Source Vertical Swinging Wood-Based Photovoltaic Racking Systems. *To Be Published*.

Yamada, T., Nakamura, H., Sugiura, T., Sakuta, K., & Kurokawa, K. (2001). Reflection loss analysis by optical modeling of PV module. *Solar Energy Materials and Solar Cells*, *67*(1), 405–413. https://doi.org/10.1016/S0927-0248(00)00309-3